Redundant Control of a Planar Snake Robot With Prismatic Joints

Motoyasu Tanaka* (iD) , Hidemasa Sawabe, Mizuki Nakajima (iD) , and Ryo Ariizumi (iD)

Abstract: This paper presents a control method of a planar snake robot with prismatic joints. The kinematic model is derived considering velocity constraints caused by passive wheels. The proposed control method based on the model allows the robot to track a target trajectory by appropriately changing its link length using prismatic joints. The degrees of freedom of prismatic joints are represented as kinematic redundancy in the model and are used in realizing subtasks such as singularity avoidance and obstacle avoidance. In addition, the link length is below its limit when introducing a sigmoid function into the kinematic model. Simulations are carried out to demonstrate the effectiveness of the proposed method and show a novel motion that avoids singular configurations through changes in link lengths.

Keywords: Snake robot, Prismatic joint, Redundancy, Kinematics, Singularity avoidance, Obstacle avoidance

Snakes move on rough terrain, across walls, and in trees even though their bodies have a simple coded shape without limbs. In addition, there are snakes that move through water and glide from trees. Snakes use a variety of types of locomotion to move in various environments. In particular, snakes use four types of locomotion to move across the ground, namely serpentine, sidewinding, rectilinear, and concertina types of locomotion [1]. Many robots have mimicked the motion of snakes [2].

The typical locomotion of a snake robot is a serpentine locomotion. A snake robot, which has a mechanism with frictional anisotropy such as a passive wheel, locomotes through undulation generated by active rotational joints. Hirose observed biological snakes and formulated a serpentine curve called the *serpenoid curve* [1]. This curve has been applied for three-dimensional motions [3, 4], such as the sinus-lifting motion. Other biomimetic approaches, such as using a central pattern generator [5, 6] and decentralized control [7], have been proposed. The main goal of these approaches is to have the robot perform the same motion as biological snakes. In contrast, using a model-based control approach to design a controller based on mathematical models of the robot, we can generate snake robot behaviors that achieve control objectives. In this approach, two models are often used: one that considers the lateral slip (i.e., skid) of wheels and one that assumes no lateral slip. In studies using a model that considers the slipping of wheels, control methods for the path

tracking of the center of mass [8] and trajectory tracking of the head [9] have been proposed. In studies using a model that assumes no slipping of wheels, a control method for the trajectory tracking of the robot's head has been proposed not only on a plane [10–12] but also on a step [13] and for two non-parallel planes [14].

Rectilinear locomotion is adopted when a large snake moves on a smooth surface, with each part of the belly of the snake repeatedly stretching and contracting [15]. The snake robot mimicking rectilinear locomotion has been researched and developed [16–20]. In [16, 17], the contact between the ground and the bottom surface of the robot was changed using the flexion of the joints to realize rectilinear motion. In [18–20], rectilinear motion was realized by sequencing the extension and contraction of the prismatic joints. An obstacle-aided locomotion method using prismatic joints and rotational joints has been proposed [20]. This motion is similar to concertina motion [21], where a snake locomotes by fixing its body parts to the surrounding terrain. In the above studies, the stretching and flexing of a robot's links mimics the stretching and flexing of the body of a living snake, and the robot locomotes through the stretching and flexing of the links.

Another example of an animal that moves by stretching and contracting is the earthworm. Earthworms adopt peristaltic movements [22]. Earthworm-like robots adopting peristaltic motion have been developed [23–25].

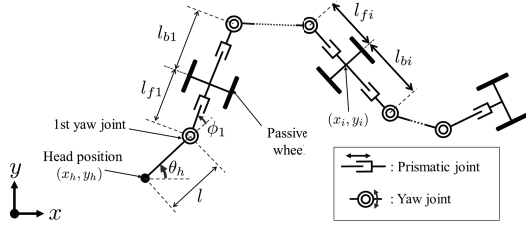In the studies mentioned above, the rectilinear motion

Fig. 1. Model of a snake robot with prismatic joints.

of a snake or peristaltic motion of an earthworm was realized through sequence control. In contrast, the three-dimensional motion of a snake robot adopting simultaneous stretching of the prismatic joints and bending of the rotational joints has been proposed [26]. In this approach, the stretching and bending are pre-scripted as a target continuous curve.

As described above, the motion of serpentine robots adopting stretching and retraction has been realized by sequence control or preliminary design. The robot is thus unable to adaptively change the link lengths according to the situation.

The present paper proposes a modeling and control method that adaptively changes the stretching and bending of a planar snake robot with prismatic joints that change the link length. The robot comprises links with passive wheels connected in series by prismatic joints and rotational joints. The robot is described as a redundant system with kinematic redundancy relating to a change in link length. The redundancy is used to adaptively change the link length. Furthermore, a sigmoid function is introduced in the model to keep the link length within hardware limitations. The effectiveness of the proposed method is demonstrated in simulations.

1. MODEL

Figure 1 shows a model of a snake robot with prismatic joints. The robot comprises rotational yaw joints, prismatic joints, and passive wheels. A link of the robot is elongated and shortened by the prismatic joint. Each link has two prismatic joints to move the passive wheels to an arbitrary position on the link. Let n be the number of rotational joints and ϕ_i be the joint angle of the ith rotational joint. The head link does not have passive wheels and has a constant length l. If the head link has passive wheels, the position and orientation of the head cannot be controlled simultaneously because of the non-holonomic constraint caused by the wheels as [11]. Thus, the head link is designed without wheels. Moreover, the prismatic joint of the head link is omitted to simplify the model. Let l_{fi} and l_{bi} respectively be the length from the ith pair of wheels to the ith rotational joint and the

length from the ith pair of wheels to the $i + 1$th rotational joint. We define $\phi = [\phi_1, \cdots, \phi_n]^\top$, $l_f = [l_{f1}, \cdots, l_{fn}]^\top$, and $l_b = [l_{b1}, \cdots, l_{b(n-1)}]^\top$. Let the position and orientation of the head be $w = [x_h, y_h, \theta_h]^\top$ and the generalized coordinate be $q = [w^\top, \phi^\top, l_f^\top, l_b^\top]^\top$.

For the robot, we set three control objectives: trajectory tracking of the robot's head, preventing the link length exceeding its limit, and accomplishment of subtasks. The snake robot without prismatic joints has a singular configuration in which the robot cannot track the target trajectory as [27,28]. As will be described later, the snake robot with prismatic joints also has a singular configuration. Thus, we adopt the avoidance of singular configuration as one of the subtasks.

Let (x_i, y_i) be the center position of the ith pair of wheels and θ_i be the absolute angle of the links connected with the ith pair of wheels. x_i and y_i are represented as

$$x_i = \begin{cases} x_h + l\cos\theta_h + l_{f1}\cos\theta_1, \ (\text{if } i=1) \\ x_h + l\cos\theta_h + \sum_{j=1}^{i} l_{fj}\cos\theta_j + \sum_{j=1}^{i-1} l_{bj}\cos\theta_j, \ (\text{if } i>1) \end{cases} \tag{1}$$

$$y_i = \begin{cases} y_h + l\sin\theta_h + l_{f1}\sin\theta_1, \ (\text{if } i=1) \\ y_h + l\sin\theta_h + \sum_{j=1}^{i} l_{fj}\sin\theta_j + \sum_{j=1}^{i-1} l_{bj}\sin\theta_j. \ (\text{if } i>1) \end{cases} \tag{2}$$

The velocity constraint of the ith pair of wheels is expressed as

$$\dot{x}_i \sin\theta_i - \dot{y}_i \cos\theta_i = 0. \tag{3}$$

Considering (3) for all pairs of wheels and time derivative of (1) and (2) yields

$$A(q)\dot{w} = B(q)u, \tag{4}$$

$$u = [\dot{\phi}^\top, \dot{l}_f^\top, \dot{l}_b^\top]^\top, \tag{5}$$

where u is the control input, the ith row of (4) represents the velocity constraint on the ith pair of wheels, and $A \in \mathbb{R}^{n \times 3}$, $B \in \mathbb{R}^{n \times (3n-1)}$. Let $B_{[i:j]}$ be the matrix comprising the $i, \cdots, j$th columns of B:

$$B_{[1:n]} = \begin{bmatrix} l_{f1} & & & 0 \\ & l_{f2} & & \\ & & \ddots & \\ * & & & l_{fn} \end{bmatrix}, \tag{6}$$

$$B_{[n+1:2n-1]} = B_{[2n+1:3n-1]} = \begin{bmatrix} 0 & \cdots & & 0 \\ b_{2,1} & & & 0 \\ \vdots & \ddots & & \\ b_{n,1} & \cdots & & b_{n,n} \end{bmatrix}, \tag{7}$$
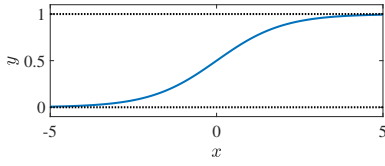
Fig. 2. Standard sigmoid function.

$$B_{[2n]} = 0, \tag{8}$$

where $b_{i,j} = -\sin\sum_{k=j+1}^{i}\phi_k$.

ϕ, l_f, and l_b have hardware limitations depending on the robot. To satisfy the hardware limitations of l_f and l_b, l_{fi} and l_{bi} are represented using a standard sigmoid function and intervening variables γ_{fi}, γ_{bi}. The standard sigmoid function (Fig. 2) is expressed as

$$f(x) = \frac{1}{1+\exp(-x)}. \tag{9}$$

Using (9), l_{fi} and l_{bi} are expressed as

$$l_{fi} = (l_U - l_L)f(\gamma_{fi}) + l_L, \tag{10}$$
$$l_{bi} = (l_U - l_L)f(\gamma_{bi}) + l_L, \tag{11}$$

where $l_U \neq 0$ and $l_L \neq 0$ are respectively the maximum and minimum values of the link length, and $l_L \leq l_{fi} \leq l_U$ and $l_L \leq l_{bi} \leq l_U$. The function used in this method is not limited to standard sigmoid functions but can be any function that increases uniformly with $-\infty \leq x \leq \infty$.

Through the differentiation of the expressions in (10) and (11) with respect to time, we obtain

$$\begin{bmatrix} \dot{l}_f \\ \dot{l}_b \end{bmatrix} = \begin{bmatrix} C_1 & 0 \\ 0 & C_2 \end{bmatrix} \begin{bmatrix} \dot{\gamma}_f \\ \dot{\gamma}_b \end{bmatrix} \tag{12}$$
$$= C \begin{bmatrix} \dot{\gamma}_f \\ \dot{\gamma}_b \end{bmatrix}, \tag{13}$$

where $\gamma_f = [\gamma_{f1}, \cdots, \gamma_{fn}]^\top$, $\gamma_b = [\gamma_{b1}, \cdots, \gamma_{bn-1}]^\top$, and

$$C_1 = (l_U - l_L)$$
$$\cdot \begin{bmatrix} \{1-f(\gamma_{f1})\}f(\gamma_{f1}) & & 0 \\ & \ddots & \\ 0 & & \{1-f(\gamma_{fn})\}f(\gamma_{fn}) \end{bmatrix}, \tag{14}$$
$$C_2 = (l_U - l_L)$$
$$\cdot \begin{bmatrix} \{1-f(\gamma_{b1})\}f(\gamma_{b1}) & & 0 \\ & \ddots & \\ 0 & & \{1-f(\gamma_{bn-1})\}f(\gamma_{bn-1}) \end{bmatrix}. \tag{15}$$

Substituting (13) into (4), we obtain

$$A\dot{w} = \bar{B}\bar{u}, \tag{16}$$

$$\bar{B} = B \begin{bmatrix} I & 0 \\ 0 & C \end{bmatrix}, \tag{17}$$

$$\bar{u} = [\dot{\phi}^\top, \dot{\gamma}_f^\top, \dot{\gamma}_b^\top]^\top. \tag{18}$$

We use (16) as the kinematic model with which to control the robot. If the link lengths l_{fi} and l_{bi} reach a maximum or minimum value, the corresponding element of C becomes zero.

2. CONTROL INPUT

The link length does not exceed its limit because the sigmoid function is used in the kinematic model (16). Thus, we design a control input to accomplish both trajectory tracking of the robot's head and subtasks. Considering the kinematic model (16), we design the input $\bar{u}$ as

$$\bar{u} = u_{\text{traj}} + u_{\text{ker}}, \tag{19}$$
$$u_{\text{traj}} = \bar{B}^{W\dagger}A\{\dot{w}_d - K(w-w_d)\}, \tag{20}$$
$$u_{\text{ker}} = -(I - \bar{B}^{W\dagger}\bar{B})K_\eta\eta, \tag{21}$$

where $\bar{B}^{W\dagger} = W^{-1}\bar{B}^\top(\bar{B}W^{-1}\bar{B}^\top)^{-1}$ is the weighted pseudo inverse matrix [29], W is the positive diagonal matrix representing weights, w_d is the target value of w, $K > 0$ is the gain related to a convergence of w, $K_\eta > 0$ is the positive diagonal matrix representing a gain related to kinematic redundancy, and $\eta \in \mathbb{R}^{(3n-1)\times 1}$ is an arbitrary vector. Substituting (19) into (16), if $\bar{B}$ is of full row rank, the closed loop system is expressed as

$$A\{\dot{w} - \dot{w}_d + K(w - w_d)\} = 0. \tag{22}$$

If A is of full column rank, w converges to w_d at $t \to \infty$. If $\bar{B}$ is not of full row rank, the closed loop system is not equal to (22) because $\bar{B}\bar{B}^{W\dagger} \neq I$.

If A and $\bar{B}$ are not of full rank, the convergence of w is not guaranteed. Such a case is called a singular configuration of the robot. At the singular configuration depending on A, all axes of grounded wheels are parallel (singular configuration I), or all extended lines of axes of grounded wheels intersect at a point (singular configuration II) [27, 28]. If $l_{fi} \neq 0$, B and $\bar{B}$ are of full row rank according to (6). Note that C does not affect the full rankness of $\bar{B}$. $\bar{B}$ is always of full row rank because $l_{fi} > 0$ through the introduction of a sigmoid function. There is thus no singular configuration depending on $\bar{B}$.

If the sigmoid function is introduced for the rotational joint, the row full rankness of $\bar{B}$ cannot be guaranteed, as shown in Appendix A.

u_{ker} in (19) is the input related to kinematic redundancy, and other control objectives (subtasks) can be achieved using u_{ker} without affecting the convergence of w. We let $V(q)$ be the cost function and design η as

$$\eta = \begin{bmatrix} \frac{\partial V}{\partial \varphi_1}, \cdots, \frac{\partial V}{\partial \varphi_{3n-1}} \end{bmatrix}^\top, \tag{23}$$

where $\varphi = [\phi^\top, \gamma_f^\top, \gamma_b^\top]^\top \in \mathbb{R}^{(3n-1)\times 1}$, and φ_i is the ith element of φ. The time derivative of V is expressed as

$$\frac{dV}{dt} = \frac{\partial V}{\partial w}\dot{w} + \frac{\partial V}{\partial \varphi}\bar{u}$$
$$= \frac{\partial V}{\partial w}\dot{w} + \eta^\top u_{\text{traj}} - \eta^\top (I - \bar{B}^{W\dagger}\bar{B})K_\eta \eta. \quad (24)$$

The third term on the right-hand side of (24) is non-positive (negative semi-definite). This means that the use of u_{ker} contributes to the reduction of V.

The controlled variables are solely the position and orientation of the robot's head, but the link length is limited by the sigmoid function. Let the cost function for singularity avoidance be V_s, the cost function for other subtasks be V_o, and V be defined as

$$V = a_s V_s + a_o V_o, \quad (25)$$

$$V_s = \frac{1}{\det A^\top A}, \quad (26)$$

where a_s and a_o are weight constants. Decreasing V contributes to the avoidance of singular configurations and the accomplishment of subtasks.

In this paper, we adopt obstacle avoidance as another subtask. We design V_o of (25) as

$$V_o = g(d_{\min}), \quad (27)$$

where $d_{\min}$ is the minimum distance between the robot and obstacle. The function g is defined as

$$g(d_i) = \begin{cases} 0 & (\text{if } d > d_o) \\ (d_i - d_o)^2 & (\text{if } d \le d_o) \end{cases} \quad (28)$$

where $d_o > 0$ is the threshold. g is a function that increases as d_i decreases, and d_i is smaller than d_o. Therefore, decreasing V_o increases the distance between the robot and obstacle, allowing the robot to avoid a collision.

When the distance between a particular point (remarkable point) on the link and an obstacle is used as a parameter of g [30], collisions between the obstacle and a non-remarkable point on the link occur more frequently as the link length increases. The minimum distance $d_{\min}$ between the whole link and obstacle is thus used.

3.　SIMULATION

Simulations are performed to verify the effectiveness of the control method, the effectiveness of the link length limitation, and the effects of changes in link length. Simulations are performed in two main environments. One simulation uses a kinematic model (4) that assumes that a wheel does not slip sideways. The other simulation uses a physics simulator that allows the wheels to slide sideways, assuming application to a real robot.
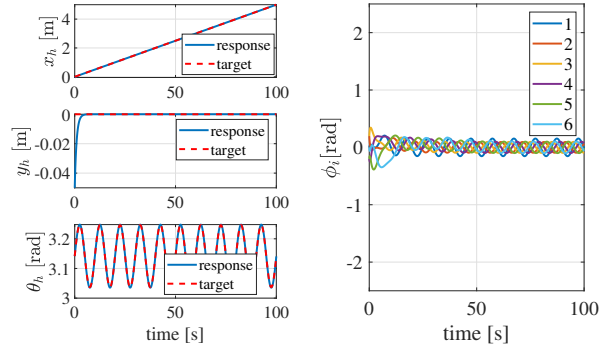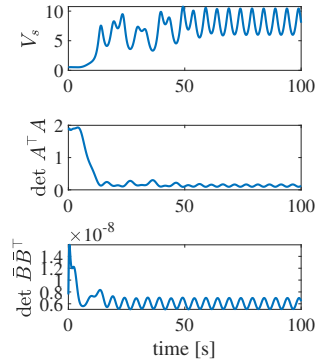

(a) w 　　　　　　(b) ϕ

(c) V_s, $\det A^\top A$, $\det \bar{B}\bar{B}^\top$

Fig. 3. Simulation results obtained using (19) without avoiding a singularity (Case 1-1, $a_s = 0$).

3.1.　Using a non-skid model

If the target path of the head is a straight line and the target posture is constant, the snake robot without prismatic joints converges to a singular configuration under the velocity constraints of the wheels [10, 11]. The robot used in this paper avoids a singular configuration by continuing to extend a link, if the link length is not limited. However, this behavior is not realistic when assuming a real robot. When the link length is limited, it is confirmed that the snake robot with prismatic joints converges to a singular configuration when a similar target trajectory is set by simulations, but the results are omitted. In previous studies of snake robots without prismatic joints, redundancy was generated in the system by introducing a link without wheels [11, 12] or lifting some wheels so that they were ungrounded [30, 31], and a singular configuration was avoided by taking advantage of the redundancy.

In contrast, the present paper proposes a novel method of avoiding a singular configuration adopting a change in link length through the use of prismatic joints. We set the target value of the head posture as a small sinusoidal
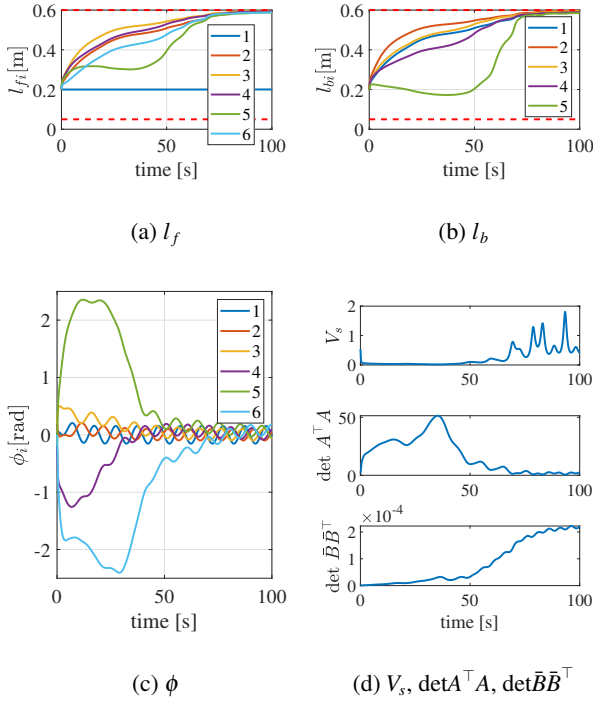
(a) l_f

(b) l_b

(c) ϕ

(d) V_s, $\det A^\top A$, $\det \bar{B}\bar{B}^\top$

Fig. 4. Simulation results obtained using (19) while avoiding a singularity (Case 1-2, $a_s = 20$, $K_\eta = I$).

(a) l_f

(b) l_b

(c) ϕ

(d) V_s, $\det A^\top A$, $\det \bar{B}\bar{B}^\top$

Fig. 5. Simulation results obtained using (19) while avoiding a singularity (Case 1-3, $a_s = 20$, $K_\eta = K_N$).

wave and expect the small vibration to be amplified by the change in link length. Note that the snake robot without prismatic joints moves with very small vibration of joint angles when using a similar target because it cannot amplify the small vibration. It means that the robot moves in a posture close to the singular configuration.

The kinematic model and controller are implemented in MATLAB. We set $n = 6$, $l = 0.1$ m, $l_L = 0.05$ m, and $l_U = 0.6$ m. The initial value of w is $w = [-0.05, -0.05, \pi]^\top$, the initial value of ϕ is $\phi = [0, \pi/16, \pi/16, -\pi/16, -\pi/16, 0]^\top$, and the initial values of all elements of l_f and l_b are 0.2 m. The target motion of the head position is a constant linear motion while the target motion of the head orientation is a minute sinusoidal wave whose amplitude is $\pi/30$.

The gain of the control input is $K = I$ and $a_o = 0$. We let the diagonal element of W be $W_1, \cdots, W_{3n-1}$ and set $W_i = 1.0$ if $1 \leq i \leq n$ and $W_i = 1.0 \times 10^5$ if $n + 1 \leq i$. The weight thus reduces the change in the link length and increases the change in the rotational joint angle. We use two types of K_η; I and K_N. We let the diagonal element of K_N be $k_{N1}, \cdots, k_{N3n-1}$ and set k_{Ni} to

$$k_{Ni} = \begin{cases} 0.001, & (\text{if } n+1 \leq i \leq 2n) \\ 1. & (\text{otherwise}) \end{cases} \quad (29)$$

In K_N, the elements corresponding to l_f are smaller than those corresponding to l_b. This means that the change in
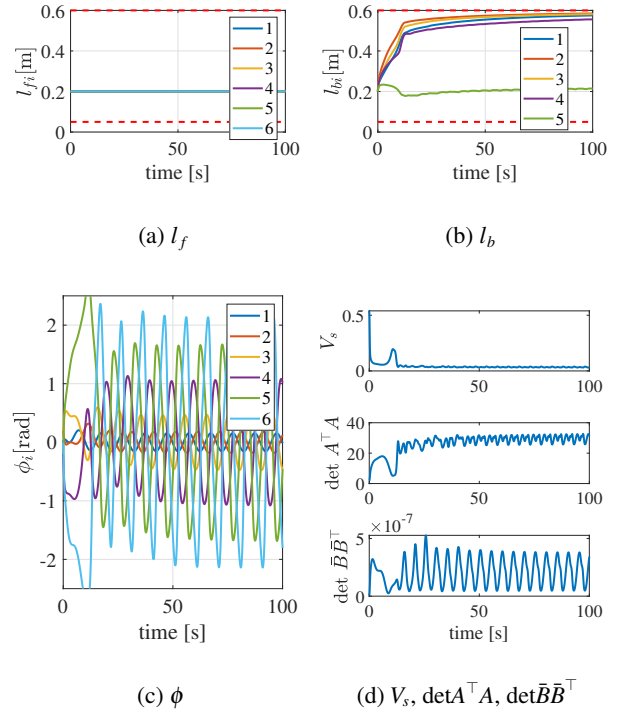
l_f when using redundancy is smaller than that in l_b.

Simulations are performed for three cases to verify the performance of singularity avoidance.

- Case 1-1: $a_s = 0$
- Case 1-2: $a_s = 20$ and $K_\eta = I$
- Case 1-3: $a_s = 20$ and $K_\eta = K_N$

If a_s is small, the link length and joint angle slowly change to avoid singular configuration because u_{ker} becomes small. It means that the effect of the singularity avoidance is small and the robot cannot obtain enough effect. In contrast, a_s is large, the effect of the singularity avoidance becomes large but the motion of the link length and joint angle becomes fast. Then, the value of $a_s = 20$ was decided by trial and error.

Figure 3 shows the results for case 1-1. w converges to the target. The link lengths l_f and l_b all remain at their initial values. This is because W is set such that the link length does not change easily and the redundant input u_{ker} is zero. $\det A^\top A$ is a value related to a singular configuration, becoming zero when the robot is in a singular configuration. Figure 3 shows that ϕ is small and $\det A^\top A$ is approximately 0.1.

Figure 4 shows the result for case 1-2, in which $a_s = 20$. w converges to the target as well as it does in Fig.3(a). Figures 4(a) and 4(b) show that l_f and l_b vary adaptively and that almost all links are finally of near-maximum length.
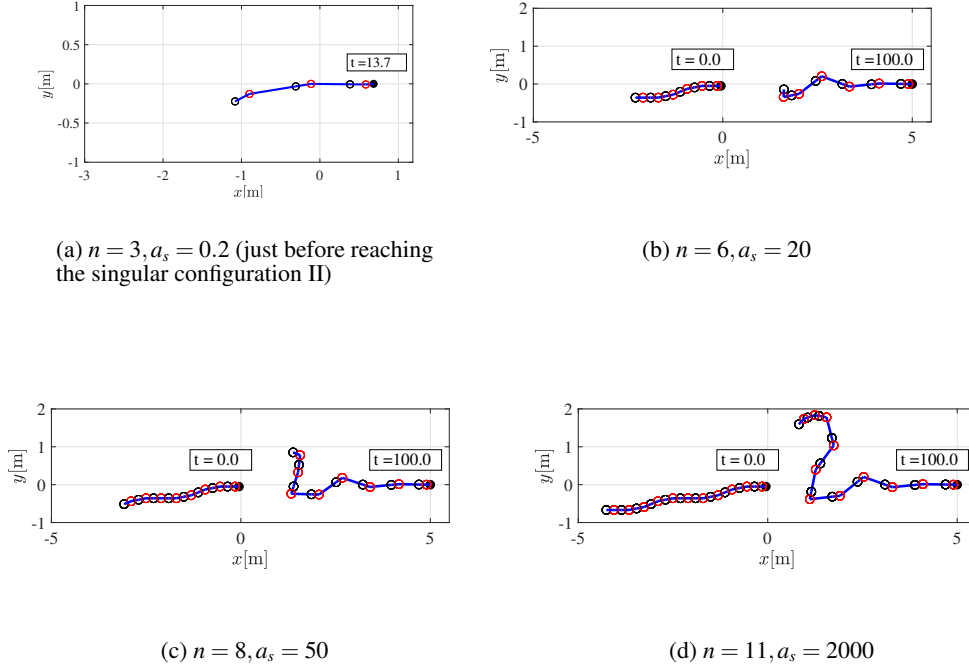
(a) $n = 3, a_s = 0.2$ (just before reaching the singular configuration II)

(b) $n = 6, a_s = 20$

(c) $n = 8, a_s = 50$

(d) $n = 11, a_s = 2000$

Fig. 6. Simulation results with avoiding a singularity ($n = 3, 6, 8, 11$).
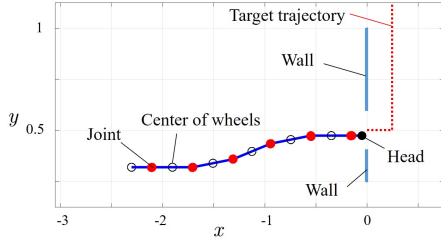
Fig. 7. Initial situation in the simulation of avoiding obstacles.

Figure 5 shows the result for case 1-3. l_f is almost unchanged from the initial state because the element of K_η corresponding to l_f is small. In contrast, l_b changes appropriately and the amplitude of the rotational joint angle ϕ increases from head to tail. The value of $\det A^\top A$ drops to 5.5 at one time but ultimately remains at approximately 28. The singularity avoidance is therefore better than that in cases 1-1 and 1-2.

The above results confirm that the robot adaptively changes its link length according to the cost function and avoids a singular configuration by amplifying the small vibration of the head orientation, and that the proposed method maintains the link length below its limit.

The minimum value of n is three because of the size of the matrix A. If $n = 3$, the robot inevitably becomes the singular configuration II as Figure 6(a). Thus, $n > 3$ should be satisfied to avoid the singular configuration. In contrast, the larger n is, the more easily the robot will amplify the vibration of the head as Fig. 6. It means that the robot is easy to avoid the singular configuration.

We next assume an obstacle-avoidance situation, such as that of Fig. 7, in which the robot passes between two walls. The distance between the walls is 0.4 m. If the outline of the robot is complex, the calculation of the minimum distance to an obstacle becomes more complicated. Therefore, assuming that the robot's link is a straight line

In addition, no link length exceeds its limit. The value of $\det A^\top A$ increases temporarily to 50 but eventually drops to approximately 2. This is a large value compared with that in case 1-1, and it can be said that the robot is able to move away from the singular configuration. The value of ϕ oscillates at a smaller value at the end of the simulation and it can be said that the result of ϕ is not much different from the result of $a_s = 0$. Although w follows the target value because of the use of a kinematic model where the wheels do not skid, if we use a real robot or model where the wheel can skid, it is expected that the resulting motion will not allow the robot to move forward because the undulation is too small.

(a) ϕ

(b) V_s, V_o, V

(c) l_f

(d) l_b

(e) $d_{\min}$

Fig. 8. Simulation results obtained using (19) without avoiding obstacles (Case 2-1, $a_o = 0, a_s = 1$).

(a) ϕ
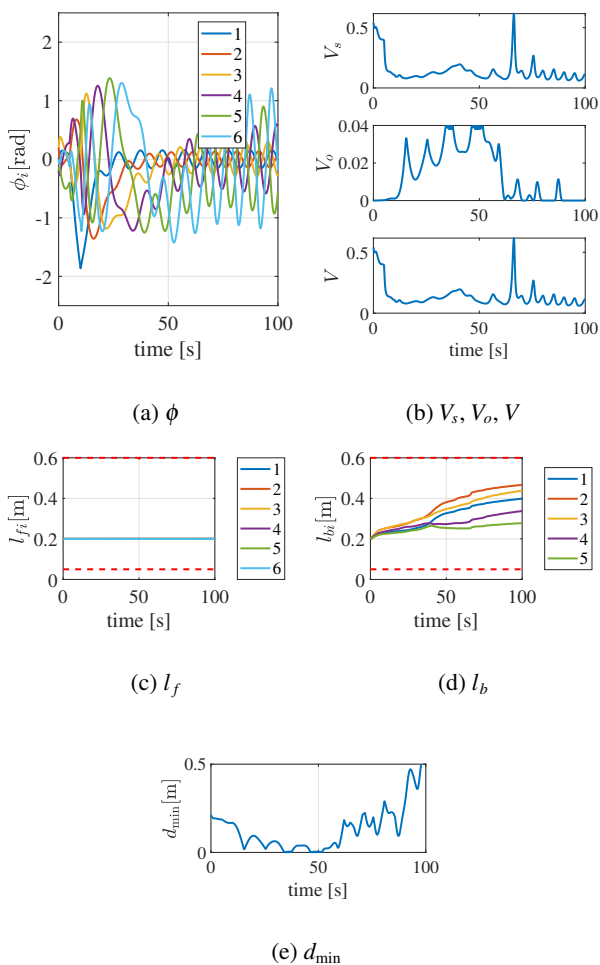
(b) V_s, V_o, V

(c) l_f

(d) l_b

(e) $d_{\min}$

Fig. 9. Simulation results obtained using (19) while avoiding obstacles (Case 2-2, $a_o = 10, a_s = 1$).

with no thickness, we calculate the minimum distance $d_{\min}$ between the robot and obstacle. We set $d_o = 0.2$, while the initial values K, K_η are the same as those in case 1-3 of singularity avoidance. The target trajectory is a $\pi/2$ turning and straight forward motion after the robot passes between the walls. We run simulations for two cases.

- Case 2-1: Obstacle avoidance is not performed ($a_o = 0$ and $a_s = 1$)
- Case 2-2: Obstacle avoidance is performed ($a_o = 10$ and $a_s = 1$)

Note that V_s and V_o are trade-off parameters depending on a_s and a_o because of (25).

Figure 8 shows the results for case 2-1. $d_{\min}$ becomes zero and the robot collides with the obstacle as shown in Fig. 8(e) because obstacle avoidance is not performed.

Figure 9 shows results for case 2-2. Figure 9(e) reveals that $d_{\min} > 0.015$m and the robot avoids colliding with the obstacle. l_f is almost unchanged from the initial state because $K_\eta = K_N$ but l_b changes appropriately as shown in
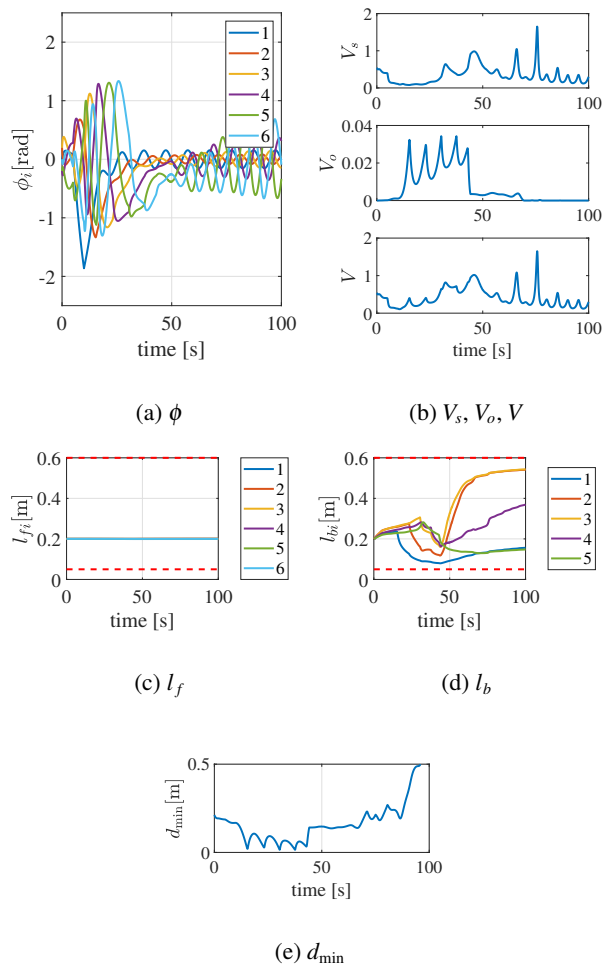
Fig. 9. The robot makes l_b so small that it avoids collisions in the neighborhood of the obstacle and has almost no lateral undulations. When the robot leaves the obstacle, it proceeds via a large undulation by enlarging l_{b2} and l_{b3}.

It is thus confirmed that the proposed method adaptively changes the link length and allows the robot to avoid obstacles. Note that obstacle avoidance may not be possible when the link length reaches its limit or if there is a trade-off with singularity avoidance.

3.2. Using a physics simulator

A physics simulator V-rep [32] is adopted to simulate singularity avoidance using a physics model in which a wheel can skid sideways. Vortex is used as the physics engine.

For singularity avoidance, it is necessary to reduce the element of K_η corresponding to $\dot{l}_f$ as described in Section 3.1. This means that the change in l_f is kept small. We therefore use the model whose l_f is constant in the V-rep simulation. Figure 10 shows the robot, while the
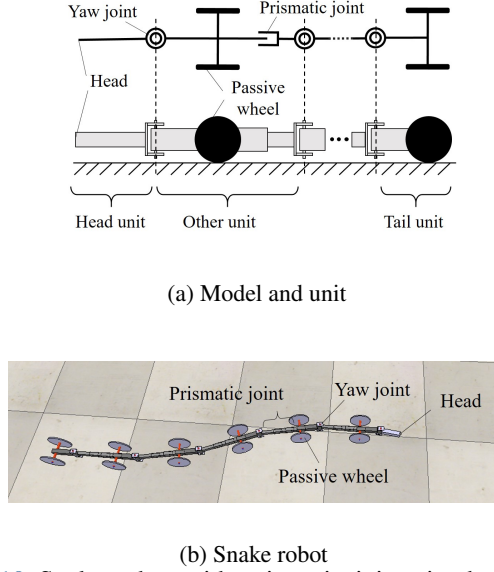
(a) Model and unit

(b) Snake robot

Fig. 10. Snake robot with prismatic joints in the V-rep simulation.

(a) w

(b) ϕ

(c) V_s, $\det A^\top A$, $\det \bar{B}'\bar{B}'^\top$

Fig. 11. V-rep simulation results without singularity avoidance ($a_s = 0$).

mathematical model and control input in this case are presented in Appendix B. We set $n = 6$, $l = 0.1$m, $l_L = 0.1$m, $l_U = 0.3$m, and $l_{fi} = 0.1$m. The weights of the head unit, tail unit, and other unit in Fig. 10(a) are respectively 86, 259, and 209 g, and the friction coefficient is 0.5. We use the target trajectory of the robot's head as in cases 1-1, 1-2, and 1-3, and we set $K = I$ and $K'_\eta = I$.

Figure 11 shows the results when $a_s = 0$ (without avoiding a singularity). The amplitude of the undulation is small and the posture of the robot is close to a straight line (singular configuration) and the controlled variables do not track the targets. If the robot moves forward when the robot is close to a singular configuration, a wheel needs to generate strong friction in the sideward direction. If the model in which the wheel does not skid is used, the robot can move forward when the robot is close to the singular configuration. However, the wheel skids in the physical simulator because there is an upper limit to the frictional force that a wheel can generate, and the robot does not move forward.

Figure 12 shows the result when $a_s = 20$ (when avoiding a singularity). The robot moves forward without converging to the singular configuration, and the controlled variables track the target trajectory. We find that the vibration of the head is amplified from the head to the tail because ϕ_i oscillates at a larger value as i increases. This is the behavior obtained when all l_{bi} converge near the maximum value.

As described above, in the case of a real robot whose wheels can skid, it is confirmed that the robot follows the target trajectory near the singular configuration and the proposed method allows the robot to follow the target tra-
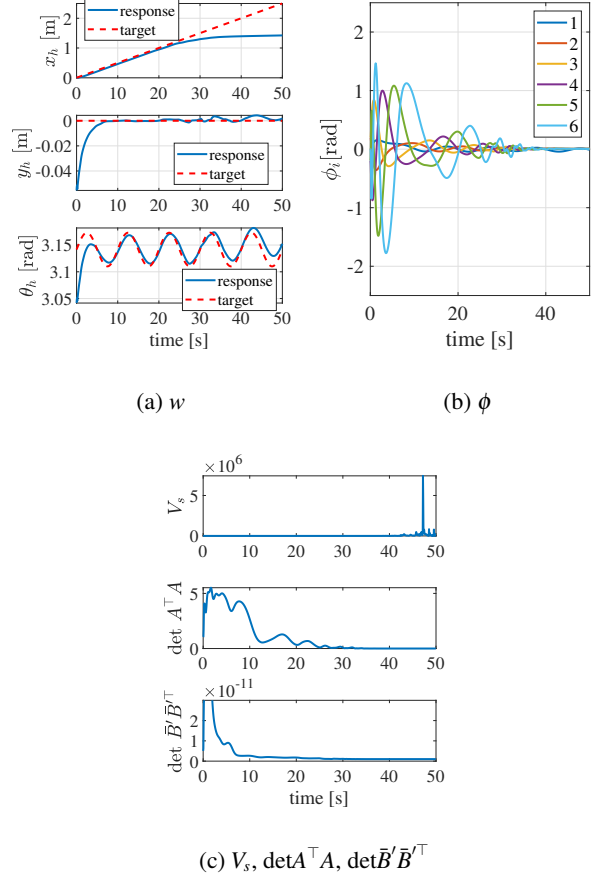
jectory while avoiding the singular configuration by amplifying the small vibration of the head.

3.3. Discussion

3.3.1 The reason why the amplitude of the undulation does not amplify when $K_\eta = I$

Focusing on the link length, the amplitude of the tail undulation increases when $l_{fi} < l_{bi}$ but decreases when $l_{fi} > l_{bi}$. If $K_\eta = I$, l_f elongates and the amplitude of the robot undulation is not amplified as seen for case 1-2 in section IV-A. A decrease in l_f means that the entire robot moves forward. Figure 13 shows two examples of decreasing l_{f1}. If $|\phi_3| > \pi/2$ as Fig. 13 (a), $|\phi_3|$ approaches $\pi/2$ as l_{f1} decreases, meaning that the robot moves away from the singular configuration. In contrast, if $|\phi_3| < \pi/2$, the magnitude of the rotational joint angle decreases because of the velocity constraints of passive wheels as seen in Fig. 13(b). This means that the robot posture approaches a straight line (i.e., a singular configuration) if l_f decreases and $|\phi_i| < \pi/2$. The situation of the simulations corresponds to the situation of Fig. 13(b) because the initial value of ϕ in simulations is smaller than $\pi/2$. The way to
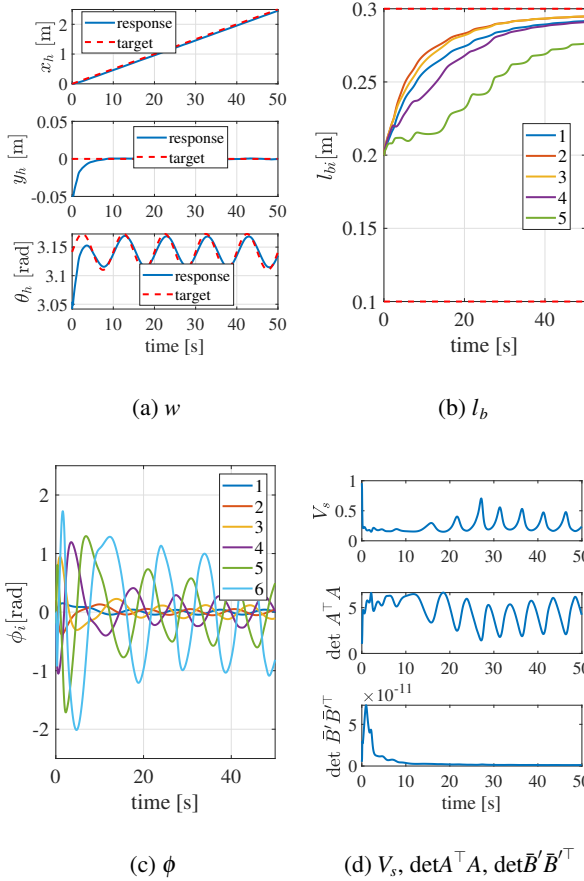
(a) w

(b) l_b

(c) ϕ

(d) V_s, $\det A^\top A$, $\det \bar{B}' \bar{B}'^\top$

Fig. 12. V-rep simulation results with singularity avoidance when $a_s = 20$.

(a)   (b)

Fig. 13. Two examples of decreasing l_{f1}: (a) $|\phi_3| > \pi/2$ and (b) $|\phi_3| < \pi/2$.

Fig. 14. Relationship between $d_{\min}$ and L_{robot} in the case 2-2.

move away from the singular configuration is to elongate l_f. Therefore, l_f continues to elongate to its maximal value to avoid singularity. However, this implies a decrease in the amplitude of the undulation and, as l_f can no longer be enlarged, the robot approaches a singular configuration. The proposed method only focuses on the gradient of a cost function that depends only on the time instant. To avoid the singular configuration with $K_\eta = I$, it is necessary to adopt an approach that considers the finite time future; for example, model predictive control.

3.3.2   Limitation of obstacle avoidance

The robot cannot move in a direction that causes a wheel to skid sideways in the kinematic model because of the velocity constraints caused by the passive wheels. In the case that the link length changes, the moving direction of the wheel and link is momentarily only the length direction of the link. This means that the robot cannot move wheels and links in the direction of velocity constraints to avoid obstacles. It is thus difficult to effectively avoid obstacles by changing link lengths. In fact, the robot does not actively move away from obstacles in the simulations
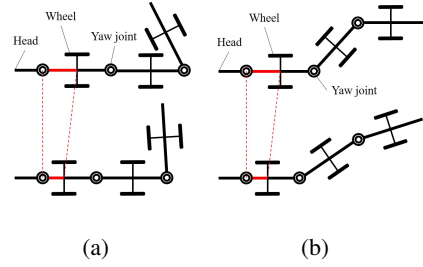
for cases 2-1 and 2-2 in section 4.1. Let L_{robot} be the total length of the robot. Figure 14 shows the relationship between $d_{\min}$ and L_{robot} in the case 2-2. $d_{\min}$ increased by the decrease of L_{robot} after $d_{\min}$ became small. Thus, the robot does move to pull the following links forward by shortening the link length so as not to undulate. We have confirmed that the motions when avoiding obstacles are similar regardless of whether the wheel does or does not skid sideways. In the case where the wheel can skid sideways, the robot moves less than the theoretical value because of slippage, and the robot undulates more to compensate for the error. It means that the risk of the collision between the robot and obstacles increases. Figure 15 shows an example of the V-rep simulation results when using the robot and simulator in the section 4.2 and using a similar target in the case 2-2. The robot came close to the obstacle at $t = 32.3[\text{s}]$ but got away from it by shortening the link length as the snapshot of $t = 34.5[\text{s}]$. In contrast, the robot approached to the obstacle again at $t = 50.9[\text{s}]$, but finally collided with it as the snapshot of $t = 52.9[\text{s}]$ because the robot could not generate the avoiding motion caused by the change of the link length.

4.   CONCLUSION

This paper proposed a method of controlling a planar snake robot with prismatic joints that change the link length. A kinematic model was derived, a controller was designed, and simulations were carried out to verify the effectiveness of the proposed method. The robot tracked

(a) Snapshots

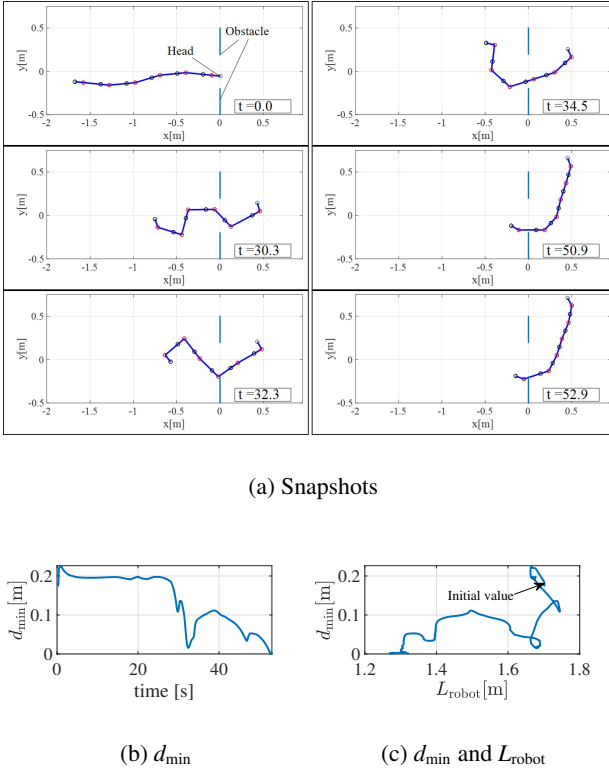(b) $d_{\min}$

(c) $d_{\min}$ and L_{robot}

Fig. 15. V-rep simulation results with avoiding obstacles using a target similar to the case 2-2.

a target trajectory by changing the link length using the proposed method. The sigmoid function was used in the model to guarantee that the link length did not exceed its limit. By changing the link length through the use of redundancy, we realized unique motions; for example, a motion for singularity avoidance in which the robot amplified a small oscillation of the head from the head to tail and a motion of obstacle avoidance.

Future works are to introduce the lifting of wheels and to conduct verification experiments using a real robot. In addition, if the robot effectively avoids a singular configuration using the proposed method, the element corresponding to l_f in K_η must be set small. This means that l_f is almost unused in accomplishing subtasks. Thus, one future work is to establish a method that allows the robot to effectively accomplish subtasks using both l_f and l_b.

ACKNOWLEDGMENTS

APPENDIX A

INTRODUCING A SIGMOID FUNCTION FOR ϕ

If a sigmoid function is introduced for the joint angle ϕ to satisfy the hardware limitation, the robot cannot generate a motion in which the velocity constraints are satisfied when the joint angle reaches a maximum or minimum value.

Using an intervening variable $\gamma_{\phi i}$, ϕ_i is expressed as

$$\phi_i = (\phi_U - \phi_L)f(\gamma_{\phi i}) + \phi_L, \tag{A.1}$$

where ϕ_U and ϕ_L are respectively the maximum and minimum joint angles. By differentiating (A.1) with respect to time, we obtain

$$\dot{\phi} = C_\phi \dot{\gamma}_\phi, \tag{A.2}$$

where $\gamma_\phi = [\gamma_{\phi 1}, \cdots, \gamma_{\phi n}]^\top$. C_ϕ is a diagonal matrix and the ith-row ith-column element of C_ϕ is $\{1 - f(\gamma_{\phi i})\}f(\gamma_{\phi i})$. Substituting (A.2) into (4), we obtain

$$A\dot{w} = B \begin{bmatrix} C_\phi & 0 \\ 0 & I \end{bmatrix} u_\phi = \bar{B}_\phi u_\phi, \tag{A.3}$$

where $u_\phi = [\dot{\gamma}_\phi^\top, \ i_f^\top, \ i_b^\top]^\top$. For the kinematic model (A.3), we design the control input as

$$u_\phi = \bar{B}_\phi^{W\dagger} A\{\dot{w}_d - K(w - w_d)\}. \tag{A.4}$$

Note that the input related to kinematic redundancy is omitted in (A.4). If A is of full column rank and $\bar{B}_\phi$ is of full row rank, the controlled variable w converges to the target w_d.

If $\phi_i(1 \le i \le n)$ reaches a maximum or minimum value, the ith-row ith-column element of C_ϕ becomes zero and C_ϕ is not of full rank. All elements of the ith column of $\bar{B}_\phi$ thus becomes zero. This means that the full column rankness of $\bar{B}_\phi$ depends on the $n+1, \cdots, 3n-1$th column of B. According to (7) and (8), all elements of the first row of $B_{[n+1:3n-1]}$ are zero. Thus, in the case that $\phi_1 = \phi_U, \phi_L$, $\bar{B}_\phi$ must be rank deficient because all elements of the first row are zero. This means that there is no guarantee of the convergence of w. In contrast, in the case that $\phi_i = \phi_U, \phi_L$ $(i \ge 2)$, $\bar{B}_\phi$ is of row full rank because of the existence of $B_{[n+1:2n]}, B_{[2n+1:3n-1]}$ by generally $\phi_U, \phi_L \neq 0$. Therefore, B is of row full rank if $\phi_L < \phi_1 < \phi_U$ and $\phi_U, \phi_L \neq 0$. If the joint angle reaches its limit, physically, the robot generates motion in which "the joint angle cannot change because the joint reaches its limit but the velocity constraints are satisfied by changing the link length."

In the case that sigmoid functions are introduced for both the joint angle and link length, the kinematic model is expressed as

$$A\dot{w} = B \begin{bmatrix} C_\phi & 0 \\ 0 & C \end{bmatrix} u_{all} = \bar{B}_{all} u_{all}, \tag{A.5}$$

where $u_{all} = [\dot{\gamma}_\phi^\top, \dot{\gamma}_f^\top, \dot{\gamma}_b^\top]^\top$.

If the joint or link length reaches its limit, C_ϕ or C is rank deficient. $\bar{B}_{all}$ is sometimes not of full row rank owing to this effect. Physically, $\bar{B}_{all}$ is rank deficient when the velocity constraint of wheels cannot be satisfied because of the limitations of the joint angle and link length.

As mentioned above, the introduction of a sigmoid function for a rotational joint angle compromises the full rankness of the matrix related to the control input and may result in cases that the convergence of w is not guaranteed.

APPENDIX B

MODEL AND INPUT WHEN L_F IS FIXED

Let us define $l_{fi} = \text{const.}(i = 1, \cdots, n)$ and replace the kinematic model with

$$A\dot{w} = B'u', \tag{B.1}$$

where $u' = [\phi^\top, l_b^\top]^\top$ and $B' = [B_{[1:n]} \quad B_{[2n+1:3n-1]}]$. Using a sigmoid function to represent a link length, we obtain

$$A\dot{w} = \bar{B}'\bar{u}' \tag{B.2}$$

$$\bar{B}' = B' \begin{bmatrix} I & 0 \\ 0 & C_2 \end{bmatrix}, \tag{B.3}$$

where $\bar{u}' = [\dot{\phi}^\top, \dot{\gamma}_b^\top]^\top$. The control input $\bar{u}'$ is designed as

$$\bar{u}' = u'_{\text{traj}} + u'_{\text{ker}} \tag{B.4}$$

$$u'_{\text{traj}} = \bar{B}'^{W\dagger} A \left\{ \dot{w}_d - K(w - w_d) \right\} \tag{B.5}$$

$$u'_{\text{ker}} = -(I - \bar{B}'^{W\dagger} \bar{B}') K'_\eta \eta', \tag{B.6}$$

where $K'_\eta \in \mathbb{R}^{(2n-1)\times(2n-1)}$ is a gain related to kinematic redundancy. $\eta' \in \mathbb{R}^{(2n-1)\times 1}$ is designed as

$$\eta' = \frac{\partial V}{\partial \varphi'}, \tag{B.7}$$

where $\varphi' = [\phi^\top, \gamma_b^\top]^\top$.

REFERENCES

[1] S. Hirose, *Biologically inspired robots: snake-like locomotors and manipulators*. Oxford: Oxford University Press, 1993.

[2] J. K. Hopkins, B. W. Spranklin, and S. K. Gupta, "A survey of snake-inspired robot designs," *Bioinspir. Biomim.*, vol. 4, no. 2, p. 021001, 2009.

[3] M. Mori and S. Hirose, "Locomotion of 3D Snake-like robots–shifting and rolling control of active cord mechanism ACM-R3–," *J. Robotics and Mechatronics*, vol. 18, no. 5, pp. 521-528, 2006.

[4] S. Toyoshima, M. Tanaka, and F. Matsuno, "A Study on Sinus-Lifting Motion of a Snake Robot With Sequential Optimization of a Hybrid System," *IEEE Trans. Autom. Sci. Eng.*, vol. 11, no. 1, pp. 139-144, 2014.

[5] A. Crespi and A. J. Ijspeert, "Online Optimization of Swimming and Crawling in an Amphibious Snake Robot," *IEEE Trans. Rob.*, vol. 24, no. 1, pp. 75-87, 2008.

[6] X. Wu and S. Ma, "CPG-based control of serpentine locomotion of a snake-like robot," *Mechatronics*, vol. 20, no. 2, pp. 326-334, 2010.

[7] T. Sato, T. Kano, and A. Ishiguro, "A decentralized control scheme for an effective coordination of phasic and tonic control in a snake-like robot," *Bioinspir. Biomim.*, vol. 7, no. 1, p. 016005, 2012.

[8] A. Mohammadi, E. Rezapour, M. Maggiore, and K. Y. Pettersen, "Maneuvering Control of Planar Snake Robots Using Virtual Holonomic Constraints," *IEEE Trans. Control Syst. Technol.*, vol. 24, no. 3, pp. 884-899, 2016.

[9] R. Ariizumi, R. Takahashi, M. Tanaka, and T. Asai, "Head-Trajectory-Tracking Control of a Snake Robot and Its Robustness Under Actuator Failure," *IEEE Trans. Control Syst. Technol.*, vol. 27, no. 6, pp. 2589-2597, 2019.

[10] P. Prautsch, T. Mita, and T. Iwasaki, "Analysis and Control of a Gait of Snake Robot," *IEEJ Trans. on Industry Applications*, vol. 120, no. 3, pp. 372-381, 2000.

[11] F. Matsuno and K. Mogi, "Redundancy controllable system and control of snake robots based on kinematic model," *Proc. 39th IEEE Conf. on Decision and Control*, Sydney, Australia, Dec. 2000, vol. 5, pp. 4791-4796.

[12] M. Tanaka and F. Matsuno, "Modeling and Control of Head Raising Snake Robots by Using Kinematic Redundancy," *J. Intell. Rob. Syst.*, vol. 75, no. 1, pp. 53-69, 2014.

[13] M. Tanaka and K. Tanaka, "Control of a Snake Robot for Ascending and Descending Steps," *IEEE Trans. Rob.*, vol. 31, no. 2, pp. 511-520, 2015.

[14] M. Nakajima, M. Tanaka, K. Tanaka, and F. Matsuno, "Motion control of a snake robot moving between two non-parallel planes," *Adv. Robot.*, vol. 32, no. 10, pp. 559-573, 2018.

[15] H. W. Lissmann, "Rectilinear locomotion in a snake (Boa occidentalis)," *J. Experimental Biology*, vol.26, no.4, pp.368-379, 1950.

[16] C. Liu and W. Liao, "A Snake Robot Using Shape Memory Alloys," *Proc. IEEE Int. Conf. on Robotics and Biomimetics*, Shenyang, China, Aug. 2004, pp.601-605.

[17] R. Primerano and S. Wolfe, "New Rolling and Crawling Gaits for Snake-like Robots," *Proc. IEEE/RSJ Int. Conf. on Intelligent Robots and Systems*, Chicago, Illinois, USA, Sep. 2014, pp.281-286.

[18] J. K. Hopkins and S. K. Gupta, "Design and modeling of a new drive system and exaggerated rectilinear-gait for a snake-inspired robot," *J. Mechanisms and Robotics*, vol. 6, no. 2, 021001, 2014.

[19] K. Wang and S. Ma, "Kinematic analysis of snake-like robot using sliding joints," *Proc. IEEE Int. Conf. on Robotics and Biomimetics*, Tianjin, China, Dec. 2010, pp.1484-1489.

[20] K. Wang, W. Gao, and S. Ma, "Snake-Like Robot with Fusion Gait for High Environmental Adaptability: Design, Modeling, and Experiment," *Applied Sciences*, vol.7, issue 11, 1133, 2017.

[21] J. Gray, "The mechanism of locomotion in snakes," *J. experimental biology*, vol.23, no.2, pp.101-120, 1946.

[22] J. Gray and H. W. Lissmann, "Studies In animal locomotion: VII. Locomotory reflexes in the earthworm," *J. Experimental Biology*, vol. 15, no.4, pp.506-517, 1938.

[23] M. Takahashi, I. Hayashi, N. Iwatsuki, K. Suzumori, and N. Ohki, "The development of an in-pipe microrobot applying the motion of an earthworm," *Proc. IEEE 5th Int. Symp. on Micro Machine and Human Science*, Nagoya Japan, Oct. 1994, pp.35-40.

[24] N. Saga and T. Nakamura, "Development of a peristaltic crawling robot using magnetic fluid on the basis of the locomotion mechanism of the earthworm," *Smart Materials and Structures*, vol.13, no. 3, 2004.

[25] N. Saga, S. Tesen, T. Sato, and J.-Y. Nagase, "Acquisition of earthworm-like movement patterns of many-segmented peristaltic crawling robots," *Int. J. Adv. Rob. Syst.*, vol. 13, no. 5, p. 1729881416657740, 2016.

[26] H. Ohno and S. Hirose, "A Study of Active Cord Mechanisms -Biomechanical Consideration on its 3D Gaits-," *J. Robotics and Mechatronics*, vol.15, no.4, pp.424-431, 2003.

[27] M. Tanaka and K. Tanaka, "Singularity Analysis of a Snake Robot and an Articulated Mobile Robot with Unconstrained Links," *IEEE Trans. on Control Syst. Technol.*, vol.24, no.6, pp.2070-2081, 2016.

[28] S. Nansai, M. Iwase, and H. Itoh, "Generalized Singularity Analysis of Snake-Like Robot," *Applied Sciences*, vol.8, issue 10, 1873, 2018.

[29] D. P. Martin, J. Baillieul, and J. M. Hollerbach, "Resolution of Kinematic Redundancy Using Optimization Techniques," *IEEE Trans. on Robotics and Automation*, vol.5, no.4, pp.529-533, 1989.

[30] M. Tanaka, K. Kon, and K. Tanaka, "Range-Sensor-Based Semiautonomous Whole-Body Collision Avoidance of a Snake Robot," *IEEE Trans. Control Syst. Technol.*, vol. 23, no. 5, pp. 1927-1934, 2015.

[31] M. Tanaka and F. Matsuno, "Control of snake robots -with switching constraints: trajectory tracking with moving obstacle," *Adv. Robot.*, vol. 28, no. 6, pp. 415-429, 2014.

[32] E. Rohmer, S. P. N. Singh, and M. Freese, "V-REP: A versatile and scalable robot simulation framework," *Proc. IEEE/RSJ Int. Conf. on Intelligent Robots and Systems*, Tokyo, Japan, Nov. 2013, pp. 1321-1326.

Motoyasu Tanaka received B.Eng., M.Eng., and Ph.D. degrees in engineering from the Department of Mechanical Engineering and Intelligent Systems, the University of Electro-Communications, Tokyo, Japan in 2005, 2007, and 2009, respectively. From 2009 to 2012, he was with Canon, Inc., Tokyo. He is currently a Professor at the Department of Mechanical and Intelligent Systems Engineering, the University of Electro-Communications. His research interests include biologically inspired robotics and dynamics-based nonlinear control. He is a recipient of the IEEE Robotics and Automation Society Japan Chapter Young Award from the IEEE Robotics and Automation Society Japan Chapter in 2006 and the Best Poster Award at SWARM2015: The First International Symposium on Swarm Behavior and Bio-Inspired Robotics in 2015.

Hidemasa Sawabe received B.Eng. and M.Eng. degrees from the Department of Mechanical Engineering and Intelligent Systems, the University of Electro-Communications in 2018 and 2020, respectively. His research interests include the development and control of snake robots.
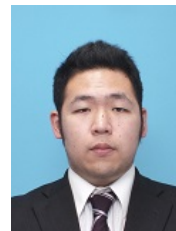
Mizuki Nakajima received B.Eng., M.Eng., and Ph.D. degrees in engineering from the Department of Mechanical Engineering and Intelligent Systems, the University of Electro-Communications in 2014, 2016, and 2020, respectively. He is currently a postdoctoral researcher at the Department of Mechanical Engineering and Intelligent Systems, the University of Electro-Communications. His research interests include the development and control of snake robots.

Ryo Ariizumi received B.Eng., M.Eng., and Ph.D. degrees from Kyoto University, Kyoto, Japan, in 2010, 2012, and 2015, respectively. He was a research fellow of the Japan Society for the Promotion of Science from 2014 to 2015. He is currently an Assistant Professor at Nagoya University, Nagoya, Japan. His research interests include the control of redundant robots and the optimization of robotic systems.